Numerical study of the thermally adaptive emissivity of VO2-polymer nanostructured coatings

Cindy Péralle, Charrière Renée, Jenny Faucheu

Numerical study of the thermally adaptive emissivity of VO_2-polymer nanostructured coatings

CINDY PÉRALLE[1,2], RENÉE CHARRIÈRE[1,*], AND JENNY FAUCHEU[1]

[1] Mines Saint-Etienne, Univ Lyon, CNRS, UMR 5307 LGF, Centre SMS, F - 42023 Saint-Etienne, France
[2] Currently with Department of Physics, Chalmers University of Technology, SE-412 96 Göteborg, Sweden
[*] Corresponding author: renee.charriere@emse.fr

Compiled March 24, 2022

The emissivity of an opal photonic crystal loaded with thermochromic VO_2 nanoparticles is studied through optical calculations. A highlight is made on the influence of the structure by comparison with a homogenized model. Parameters are first set to maximize the structure influence on the material emissivity. Then, a full study of the influence of the VO_2 concentration is made in order to identify, on one hand, cases with the highest structure impact, and on the other hand, interesting cases for applications like energy-efficient coatings for buildings, satellites and camouflage applications.

http://dx.doi.org/10.1364/ao.XX.XXXXXX

1. INTRODUCTION

Vanadium dioxide (VO_2) has drawn large interest because of its phase transition from semiconducting to metallic at a characteristic temperature of 68°C, followed by a change of its optical and physical properties. In particular, VO_2 exhibits an emissivity change linked to its phase transition in a wide wavelength range from about 3 µm to 30 µm. Its emissivity decreases abruptly when its temperature goes from below to above the transition temperature [1]. This emissivity drop is interesting for adaptive infrared camouflage applications [2–5]. When deposited onto a highly infrared reflective substrate, the emissivity switch of a VO_2 containing material can be reverted [6]. This reverted switch can be useful for dynamic radiative cooling [7–10] or for the thermal control of spacecrafts [11, 12]. Ono et al. [13] demonstrated that it is possible to choose the sign of the switch by modifying the resonance wavelength of the dielectric function of the top layer in a structure composed of a metallic substrate and an intermediate layer containing VO_2 nanoparticles. $Ge_2Sb_2Te_5$ is another phase-changing material whith tunable emissivity [14] which can be used for thermal camouflage [15]. But, contrary to VO_2, this material requires an annealing process to initiate the phase change.

A high emissivity means that the material surface radiates a large amount of thermal energy. At high temperatures, this property can be used to regulate the temperature inside buildings and satellites, as the incoming light absorbed at the wall surface is largely emitted before its propagation through the material by thermal conduction. At lower temperatures, a lower emissivity is preferred to allow more thermal energy to heat the other side of the material. So for thermal control of buildings or satellites, an emissivity increase with the temperature is desired. On the contrary, the opposite behavior is desired for adaptive infrared camouflage applications. To appear less visible on an infrared camera, a body needs to always radiate a similar amount of thermal energy as its surroundings. Usually, the background has a low temperature and thus, according to Stefan–Boltzmann law [16], emits a small amount of energy. The body thus needs to emit few radiations, even when it gets hot. Thus it has to have a small emissivity, particularly at high temperatures. So an emissivity decrease at the phase transition would be preferred in this case.

In the case of an opaque material a change of emissivity can be obtained by a change of the material reflectance: a high mid-infrared reflectance leads to low emissivities. Note that a material can be transparent in the visible/near-infrared wavelength range (from about 400 nm to 3 µm) and be opaque in the mid-infrared wavelength range (from about 3 µm to 30 µm). Various VO_2-based systems with low emissivities were proposed by adding to VO_2 highly mid-infrared reflective layers: an Al substrate [6], a Pt top layer [17], an architecture with an Ag layer and antireflection stack [18]. Another approach to increase the mid-infrared reflectance, and thus reduce the emissivity, is by introducing a material nanostructuration. Square arrays [11], slit arrays [19], periodic trapezoidal multilayers [9] or cones [10] were shown to exhibit interesting emissivity properties.

The numerical study presented in this paper aims at building recommendations for further studies related to VO_2 based materials. Indeed, variety of elaboration routes have been explored and several experimental results and calculations indicate that nanocomposites containing VO_2 nanoparticles embedded in a dielectric matrix such as polymers have superior properties than VO_2 continuous thin films [20]. Also, industrially-scalable flexible polymer opals containing nanoparticles can be produced

at low cost [21], and in particular lower cost than thin films requiring vacuum deposition techniques. They present interesting optical properties [22] due to a Photonic BandGap (PBG) effect [23] generating a reflectance peak whose size and position are controllable. Polymer opals with various compacities and nanoparticle concentrations can be synthesized through self-assembly techniques using core-shell latex with a hard core and a flexible shell. The nanoparticles are embedded, with a controllable concentration, in the shell which fills the interstices after filmification. The compacity of the structure is controllable by modifying the ratio between the shell and the core diameters. The present paper is thus focused on the optical properties of an opal photonic crystal loaded with VO_2 nanoparticles. It is studied through optical calculations using the Fourier Modal Method (FMM) [24] through the MC Grating commercial software [25] coupled with a home-made program. The influence of the nanostructure is studied through comparisons between a model considering the opal nanostructure and its homogenized counterpart using a Maxwell-Garnett (MG) approximation [26]. The MG approximation gives the refractive index of a mixture of nanoparticles inside a medium and assumes that the nanoparticles are far enough from each other to neglect the interaction between them. Structural parameters are chosen in order to optimize the influence of the structure on the material emissivity, then a set of optimized parameters is proposed for each selected application (camouflage or thermal control).

2. MODEL DESCRIPTION

A. Definition of the material emissivity

To quantify the coating performances towards the considered applications, the material emissivity ϵ is calculated as:

$$\epsilon = \frac{\int (1 - R(\lambda) - T(\lambda)) M_\lambda(\lambda, \tau) d\lambda}{\int M_\lambda(\lambda, \tau) d\lambda}, \quad (1)$$

with R(λ) and T(λ) respectively the material spectral reflectance and transmittance at the wavelength λ, and $M_\lambda(\lambda, \tau)$ the blackbody spectral emittance at a temperature τ at the wavelength λ derived from Planck's law. This formula computes the total hemispherical emissivity. Despite the anisotropy of the opal structure, an angularly resolved emissivity is not considered here, as the paper is focused on applications like thermal camouflage or energy saving building coatings where the material performances are principally characterized by the total hemispherical emissivity. The emissivity modulation $\Delta\epsilon$ is then calculated as the emissivity difference between the cold and warm conditions:

$$\Delta\epsilon = \epsilon_{cold} - \epsilon_{warm}. \quad (2)$$

ϵ_{cold} and ϵ_{warm} are computed by considering the reflectance and transmittance values obtained respectively for the VO_2 cold and warm phases refractive indexes (see Fig. 2). For both ϵ_{cold} and ϵ_{warm} a temperature of $\tau = 70$°C is considered for the blackbody spectral emittance. A unique temperature has been chosen to have general results not depending on different blackbody temperatures. This temperature is very close to the VO_2 phase transition (68°C). Also, the expected influence of the blackbody temperature is low, as a variation of for example ±50°C of its temperature leads to a variation of only about ±1.5 µm of the blackbody emittance peak (see Eq. 4), with the blackbody emittance peak having a wide shape, with a full width at half maximum of about 10 µm at 70°C [16].

B. System description

A 3D opal photonic crystal loaded with VO_2 spherical nanoparticles is modeled using the FMM combined with a staircase approximation [27] to model the third dimension (z direction in Fig. 1). Polymer spheres, labeled P_s are arranged in an fcc-lattice with a cell parameter a. The interstitial spaces are filled with VO_2 spherical nanoparticles dispersed in another polymer labeled P_i. The system is surrounded by air on both sides. The light is normally incident on the sample surface and is thus along the crystallographic [111] direction. A schematic representation of a vertical cross-section of the system upper part is given in Fig. 1a.

The model used in this work considers homogenized interstices modeled by an effective refractive index derived from a MG approximation, considering VO_2 spherical inclusions in the P_i polymer medium (see Fig. 1b). In order to study the impact of the structure on the material optical properties, a second MG approximation is used to model a completely homogenized layer, considering the P_s polymer spherical inclusions surrounded by the interstices homogenized material (Fig. 1c).

The thermochromic property of VO_2 is modeled by two refractive indexes in each cold and warm conditions. These refractive indexes in the visible and near infrared regions ([350 nm - 2500 nm]) are extracted from [28], while the ones in the mid-infrared region ([2500 nm - 30000 nm]) are extracted from [6]. Fig. 2 represents the real and imaginary parts of the VO_2 refractive index in the whole wavelength range [350 nm - 30000 nm] in both cold and warm conditions with a 21.5 nm step linear interpolation below 2500 nm and a 500 nm step above.

C. Parameters setting

C.1. Setting the cell parameter

From the objective of maximizing the structure impact (and thus the PBG impact) on the material emissivity comes a few conditions on the material structural parameters. First of all, because the emissivity is obtained through an absorptance weighted by the blackbody spectral emittance (see Eq. 1), it seems interesting to align the crystal PBG peak with the blackbody emittance peak. On one hand, the PBG peak position λ_{PBG} can be estimated using Bragg's law [29] :

$$\lambda_{PBG} = 2 d_{111} \Re\left(\sqrt{n_{eff}^2 - \sin^2(\theta)}\right) \quad (3)$$

with d_{111} the distance between the (111) planes, n_{eff} the material effective refractive index and θ the light incidence angle with respect to the normal of the sample surface. If c is a complex number, $\Re(c)$ is the real part of c.

On the other hand, the position of the blackbody emittance peak λ_{BB} can be obtained through the Wien's law [16]:

$$\lambda_{BB} = \frac{A}{\tau} \quad (4)$$

with $A = 2.897771955.10^{-3}$ m.K and τ the material temperature. Equalizing λ_{PBG} with λ_{BB} leads to both peaks aligned at a wavelength of 8.44 µm, considering as a first estimation a system composed of a compact opal with polymer spheres of refractive index $n(P_s) = 1.3$ with interstices filled with pure cold VO_2. n_{eff} is thus computed through MG approximation considering spherical inclusions of refractive index $n(P_s) = 1.3$ with a 74 vol% concentration in a matrix of pure cold VO_2. The light incidence angle is $\theta = 0°$ and the temperature $\tau = 70$°C. Placing the PBG at 8.44 µm leads to a cell parameter $a = d_{111}\sqrt{3} = 4.5$ µm.

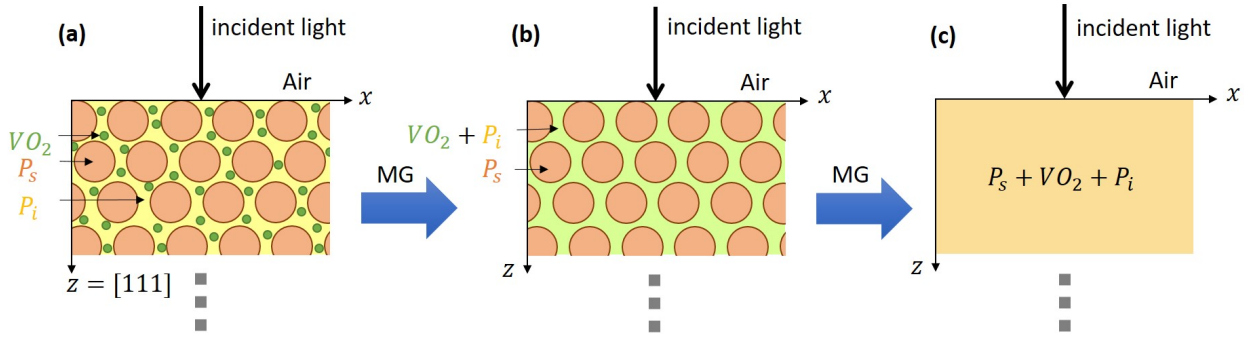

Fig. 1. Schematic representation of a vertical cross-section of an opal photonic crystal : (a) loaded with VO_2 nanoparticles, (b) where the opal interstices are homogenized and (c) when the whole material is homogenized. Only the region near the material surface is represented. MG approximations are used for homogenization processes.

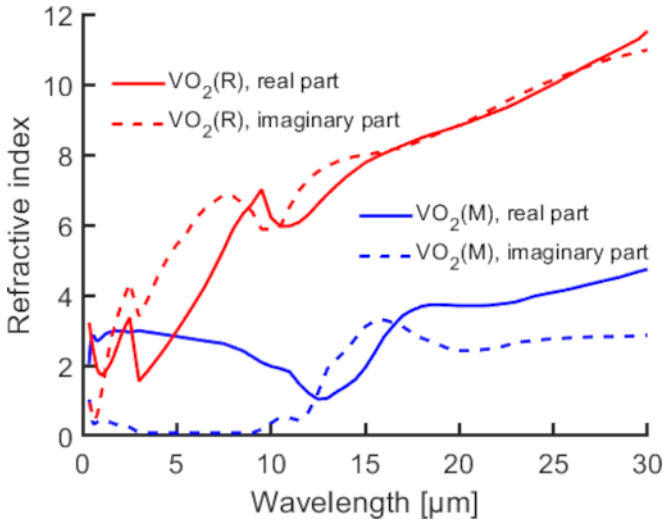

Fig. 2. Real and imaginary parts of the VO_2 refractive index in both cold (VO_2(M) phase) and warm (VO_2(R) phase) conditions. The values are extracted from [28] in the [350 nm - 2500 nm] wavelength range, and from [6] in the [2500 nm - 30000 nm] wavelength range.

C.2. Setting the polymers refractive index

Then, for a maximized PBG effect, a high refractive index contrast between the opal spheres and the interstices is desired at the PBG wavelength [23]. While the spheres refractive index is directly related to the refractive index of the polymer P_s, the interstices refractive index combines the refractive indexes of both VO_2 and the polymer P_i. Noticing that in the considered spectral region, the real part of the VO_2 refractive index is higher than those of common polymers (typically between 1.3 and 1.7), this translates into an increase of the interstices refractive index with increasing VO_2 quantities in the system. Finally, maximizing the index contrast results in minimizing P_s refractive index ($n(P_s)$ = 1.3) and maximizing P_i refractive index ($n(P_i)$ = 1.7).

C.3. Setting the staircase approximation resolution

In the FMM, the model cell is built through stacked layers along the [111] direction. The number of layers/period determine the spatial resolution that needs to be optimized regarding both computation time and correct modeling of the sphere shapes. In order to optimize the spatial resolution, models having 48, 72, 120 and 168 layers/period were considered and used to calculate the material spectral reflectance for normally incident light. Note that a period in the [111] direction is equal to $d_z = 3d_{111} = a\sqrt{3}$. Then, the normalized root mean square of the difference between one reflectance spectrum and the reflectance spectrum for 168 layers/period has been computed. The root mean square difference decreases slightly for resolutions higher than 72 layers/period (see Supplemental document for details). It has been thus decided to use a resolution of 120 layers/period as a best compromise between spatial resolution and computation time.

C.4. Setting the number of periods in the [111] direction

Now that the model spatial resolution is set, the next parameter to consider is the material thickness. For this study, five values were considered for the total number of periods in the [111] direction: 1, 3, 5, 7 and 15. As the number of periods increases, the optical behavior of the material should get closer to the behavior of an infinite crystal which has a perfect photonic bandgap (no light entering the material, which corresponds to a value of 1 for the reflectance). The closer to this infinite crystal the material gets, the more well-defined the PBG becomes, with a maximum reflectance amplitude. The purpose is here to choose the minimum number of periods to have a material behavior similar to an infinite crystal. Spectral reflectances were calculated for each number of periods, in cold condition.

Besides the case of 1 period, the reflectance variations related to variations of the number of periods are limited (see Supplemental document for details). We could thus consider a very thin material with for example three periods along the [111] direction, as the reflectance spectra barely changes with higher number of periods. However, we would like to later consider lower VO_2 concentrations. Reducing the VO_2 concentration may lead to a more transparent material, meaning that the light would then be able to reach deeper layers, thus increasing the influence of these deeper layers. It has thus been decided to consider 15 periods in the later simulations. It corresponds to a material thickness of 117 µm, which is also reasonable compared to usual thicknesses of polymer paints.

3. RESULTS AND DISCUSSION

The optical properties (reflectance, transmittance, emissivity) of the material were computed in the wavelength range [350 nm - 30000 nm] for different values of the total VO_2 concentration in the material f_t, as well as for different values of the structure compacity C. The structure compacity is given by the following

formula:

$$C = 4 \times \frac{\frac{4}{3}\pi r^3}{a^3}, \quad (5)$$

with a the cell parameter of the structure and r the spheres radius. As the cell parameter is fixed (see section C.1), changing the structure compacity is obtained by changing the spheres radius. For f_t below 26 vol%, the structure is always compact, which corresponds to a compacity $C = 0.74$. A concentration modification is obtained by changing the VO_2 concentration in the interstices. The interstices are thus in this case a mix of VO_2 and the polymer P_i. For f_t above 26 vol%, a concentration modification is obtained by changing the opal spheres size, thus modifying the structure compacity. Above $f_t = 26$ vol%, it is indeed necessary to decrease the structure compacity in order to increase f_t, as $f_t = 26$ vol% corresponds, for a compact structure, to the case where interstices are completely filled with VO_2. Above $f_t = 26$ vol%, a mixed influence of both variations of f_t and C will thus be observed. To show the influence of the compacity only, an additional study has been performed: f_t is fixed to 26 vol% while C varies. The fixed value of f_t is obtained by changing the VO_2 interstices concentration f_i according to the following formula:

$$f_i = \frac{f_t}{1 - C}. \quad (6)$$

The following sections will first present the reflectance and transmittance spectra of the material for the cold and warm phases of VO_2. Then, the emissivity will be computed from the reflectance and transmittance spectra (see Eq. 1). The material optical properties are calculated for 12 different combinations of total VO_2 concentration and compacity values (see Table 1). Table 1 also indicates the VO_2 interstices concentration f_i in all cases.

Table 1. Compacity C, total VO_2 concentration f_t and interstice VO_2 concentration f_i values used to compute the material optical properties. f_i is indicated as values in vol% inside the table.

f_t [vol%] \ C	0.74	0.48	0.22	0.01
1	3.85			
5	19.23			
10	38.46			
15	57.69			
20	76.92			
26	100	50	33.33	26.26
52		100		
78			100	
99				100

A. Reflectance and transmittance spectra

This section is split into three subsections concerning different ranges of the VO_2 total concentrations : [1, 20] vol% for the first one, 26 vol% for the second one and [26, 99] vol% for the third one.

A.1. VO_2 total concentrations from 1 to 20 vol%

Let us first consider the lower VO_2 concentrations (1, 5, 10, 15 and 20 vol%). Fig. 3 represents the reflectance and transmittance spectra for the polymer opal and its homogenized counterpart in cold and warm conditions. The reduced VO_2 concentration is followed by a reduced absorption in the material. We link here the absorption property of the material to the Beer-Lambert-Bouguer's law [30–32] and to the absorption coefficient $\alpha = 4\pi\Im(n(\lambda))/\lambda$, with $\Im(n(\lambda))$ the imaginary part of the material refractive index n at a wavelength λ. This is confirmed by the decrease of the effective refractive index imaginary part for the interstices (Fig. S3 a)-b)) and for the fully homogenized material (Fig. S4 a)-b)). This leads to two main observations: the first one is that at low enough concentrations and at certain wavelengths, the material becomes partially transparent. This can be seen on the non-zero values of the transmittance spectra (see Fig. 3 c)-d)-g)-h)), but also in the presence of oscillations in the transmittance and reflectance spectra due to thin film interferences, as the light reaches the backside of the material (see Fig. 3 a)-b)-e)-f)).

The second observation is that the PBG reflectance peak (peak between 7 μm and 8 μm in the cold condition, and between 7 μm and 14 μm in the warm condition) can be observed in both the cold and warm conditions as the absorption is weak enough to see the influence of the structure on the material optical properties. The good agreement of this peak's position and the Bragg's law (see Fig. S5) confirms that it corresponds actually to the PBG. The PBG reflectance peak corresponds to a transmittance hole, which is particularly visible for low VO_2 concentrations where the material is transparent enough. In both cold and warm conditions, as the VO_2 concentration increases, the PBG reflectance peak amplitude decreases and the peak position shifts towards longer wavelengths. In the cold conditions, this peak located at a wavelength of 7.3 μm at f_t = 1 vol% shifts to 8 μm for f_t = 20 vol%. In the warm conditions, the peak both shifts and enlarges, changing from a sharper peak centered in 7.3 μm when f_t = 1 vol% to a smoother peak extending from 8 to 15 μm, with a maximum value at a 7.2 μm wavelength when f_t = 20 vol%. A second peak starts to be apparent on the left of the PBG peak for f_t above 10 vol%, which corresponds to a higher order photonic band effect effect due to the periodic structure. The peak amplitude decrease is due to the material higher absorption coefficient, with a stronger decrease in the warm condition due to higher absorption of the warm VO_2 phase compared to the cold one around the PBG position (see the imaginary parts of the VO_2 (M) and VO_2 (R) refractive indices in Fig. 2, as well as interstice and homogenized effective refractive indices in Fig. S3 a)-b) and Fig. S4 a)-b)). Note that a decrease of the PBG reflectance peak could be due to a decrease of the refractive index contrast between the interstices and the spheres. This is not the case here, as it can be observed in Fig. S3 a)-b): the real part of the interstice effective refractive index increases with the VO_2 concentration, leading to an increase of the refractive index contrast. This increase of the refractive index contrast, which is particularly important in the warm condition, explains the widening of the PBG peak when f_t increases.

The peak position shift is due to a higher effective refractive index for the completely homogenized material, which according to Bragg's law (see Eq. 3), leads to a red-shift of the peak (see Fig. S4 a)-b)). Note that the PBG reflectance peaks (as well as the corresponding transmittance holes) are not present in the homogenized cases. Other reflectance peaks at wavelengths lower than the PBG can be observed, also not present in the corre-

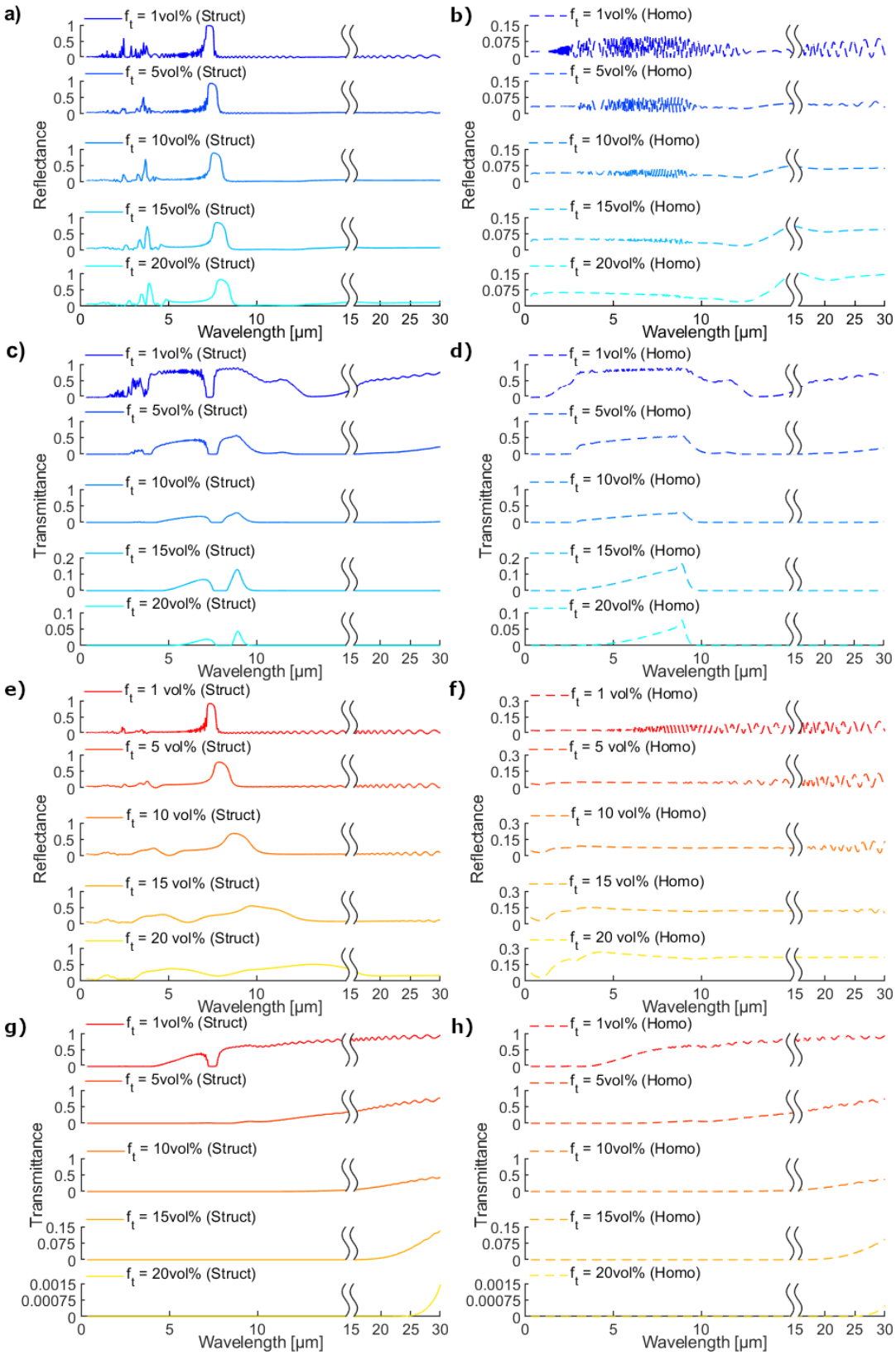

Fig. 3. Reflectance (a), b), e), f)) and transmittance (c), d), g), h)) spectra of a compact ($C = 0.74$) polymer opal photonic crystal consisting of polymer spheres ($n(P_s) = 1.3$) surrounded by a mixture of VO_2 and another polymer ($n(P_i) = 1.7$) (solid lines, designated by "struct"), and its homogenized counterpart (dashed lines, designated by "homo"), in cold (a), b), c), d)) and warm (e), f), g), h)) conditions, for a VO_2 total concentration from 1 vol% to 26 vol% (see Table 1 for the corresponding interstice concentrations). For the sake of clarity the homogenized cases are represented in separate graphs and the x-axis has been broken at a wavelength of 15 μm, to see more clearly the shortest wavelengths. Note also that the vertical scale is not the same for all graphs.

sponding homogenized cases. They correspond to higher orders photonic band effects. Corresponding transmittance holes can be observed in the cold condition for the structured case, particularly at the lowest VO_2 concentrations.

A.2. VO_2 total concentration of 26 vol%

Let us now focus on the cases where the total VO_2 concentration is equal to 26 vol% with the structure compacity varying (see Fig. 4). In the cold condition, a decrease of the compacity leads to a decrease of the PBG and higher order reflectance peaks as well as to a shift of the PBG peak towards longer wavelengths. The decrease of the peak is here not due to an increase of the material absorption. It can be seen in Fig. S3 c) and Fig. S4 c) that both the interstice and homogenized material effective refractive index imaginary parts decrease with the compacity. The decrease of the PBG peak can be partly explained by a decrease of the refractive index contrast between the interstice and the spheres (see Fig. S3 c)). This decrease is also due to the modification of the compacity: a material with very small compacity is close to a homogeneous material and thus has a very small PBG peak. The cases $C = 0.22$ and $C = 0.01$ have similar values of the interstice effective refractive index (see Fig. S3 c)) but the case $C = 0.01$ does not exhibit a PBG peak whereas the case $C = 0.22$ has a clearly visible PBG peak. As previously observed in subsection A.1, the PBG and higher order reflectance peaks aren't visible in the homogenized cases. Also, the very weak influence of the structure in the case $C = 0.01$ leads to almost similar spectra for the structured and homogenized cases.

The shift of the PBG peak position is due to an increase of the real part of the homogenized material effective refractive index around the PBG position (see Fig. S4 c)), as previously seen in subsection A.1.

In the warm condition, at the maximum compacity, no PBG peak is observed, due to the high absorption of the material (see Fig. S3 d) and Fig. S4 d) respectively for the interstice and homogenized material effective refractive indices). The interstices are composed of pure VO_2 in this case (see Table 1). The high absorption of the interstices leads to a high absorption of the global material. The homogenized case is close to the structured case besides around 2.5 μm where the structured case exhibits lower values. This could be explained by a residual structural effect appearing at low wavelengths, where the material absorption is the smallest. Then, at compacity values of $C = 0.48$ and $C = 0.22$ the PBG peak is present, and its amplitude decreases with increasing compacity. Similarly to the cold condition, the decrease of the PBG peak is partly due to a decrease of the refractive index contrast between the spheres and the interstices (see Fig. S3 d)), as well as to the decrease of the compacity. No shift of the PBG peak position is observed here, which is explained by the very small variations of the effective refractive index of the homogenized material for compacities lower than $C = 0.48$ (see Fig. S4 d)). In the case $C = 0.01$, the structure has a negligible impact, with the structured and homogenized cases having almost the same values.

Regarding the transmittance, it remains very low for both the cold and warm conditions, and particularly for the cold condition. In the cold condition, the transmittance has non-zero values in the wavelength range [3 μm - 10 μm]. This range corresponds to the wavelength range where the interstice and homogenized material effective refractive index imaginary parts (and thus the material absorption) are the smallest (see Fig. S3 c) and Fig. S4 c)). The transmittance increases when the compacity decreases, due to the reduction of the material absorption for decreasing compacity. When comparing structured and homogenized cases, it can be observed that, besides for the smallest compacity, the structured case transmittance is always lower than the homogenized one, which is due to the impact of the structure which induces reflectance peaks in this wavelength range. Also, a drop of the transmittance can be observed respectively at about 8 μm, 8.5 μm and 9 μm for $C = 0.74$, $C = 0.48$ and $C = 0.22$: this corresponds to the transmittance hole linked to the reflectance PBG peak. This is confirmed by the good agreement between this hole position and the Bragg's law (see Fig. S5).

In the warm condition, the transmittance has non-zero values for compacities lower than $C = 0.48$, for wavelengths higher than about 20 μm or 15 μm depending on the compacity. As previously observed in the cold condition, the transmittance increases when the compacity decreases, due to the decrease of the material absorption (see Fig. S3 d) and Fig. S4 d)). As the material is transparent enough to have light reaching its backside, thin film interferences oscillations can be observed at compacities below $C = 0.48$ (the oscillations are barely visible for $C = 0.48$). Note that these oscillations are also visible in the reflectance spectra. When comparing the structured and homogenized cases, the transmittance spectra are very close to each other for all compacities, due to the weaker influence of the structure for wavelengths higher than the PBG. This can be explained by looking at the photonic band structure of an fcc structure (see for example Chapter 6 of [23]) where it can be seen that for frequencies below the PBG (that is for higher wavelengths), only one linear band is observed, corresponding to the behavior of a homogeneous material. Note that this remark is applicable to all reflectance and transmittance spectra: the main differences between homogenized and structured cases are always observed at wavelengths around or smaller than the PBG position.

It can be noticed that despite the constant total VO_2 concentration, the reflectance and transmittance in the homogenized case does not remain constant as a function of the compacity. This is due to the modification of the volume fraction of refractive indexes 1.3 (refractive index of the polymer spheres $n(P_s)$) and 1.7 (refractive index of the polymer mixed with VO_2 in the interstices $n(P_i)$) (see subsection C.2). For example, when the compacity is $C = 0.74$, the volume fraction of $n(P_s) = 1.3$ is 74 vol% and the volume fraction of $n(P_i) = 1.7$ is 0 vol%. When the compacity is $C = 0.01$, the volume fraction of $n(P_s) = 1.3$ is 1 vol% and the volume fraction of $n(P_i) = 1.7$ is 73.74 vol%.

A.3. VO_2 total concentrations from 26 to 99 vol%

The last cases considered in this study correspond to total VO_2 concentrations f_t from 26 to 99 vol% (see Fig. 5). First considering only the dashed lines (completely homogenized layer), an increase of VO_2 concentration leads to an increase of the material spectral reflectance for both cold and warm conditions. It is related to an increase of the refractive index difference at the interface between the material and the surrounding air (see Fig. S3 e) and Fig. S4 f)).

Then, comparing these curves with the solid lines highlights the impact of the structure. The structure has a low impact in the cold condition for wavelengths higher than 10 μm for all values of f_t. For wavelengths below 10 μm, it can be observed that the PBG and higher order reflectance peaks decrease in amplitude as f_t increases, with no more visible impact of the structure for $f_t = 99$ vol%. The is due to a combined effect of the increase of the material absorption (see Fig. S4 e)) and the decrease of its compacity. A shift of the PBG peak toward

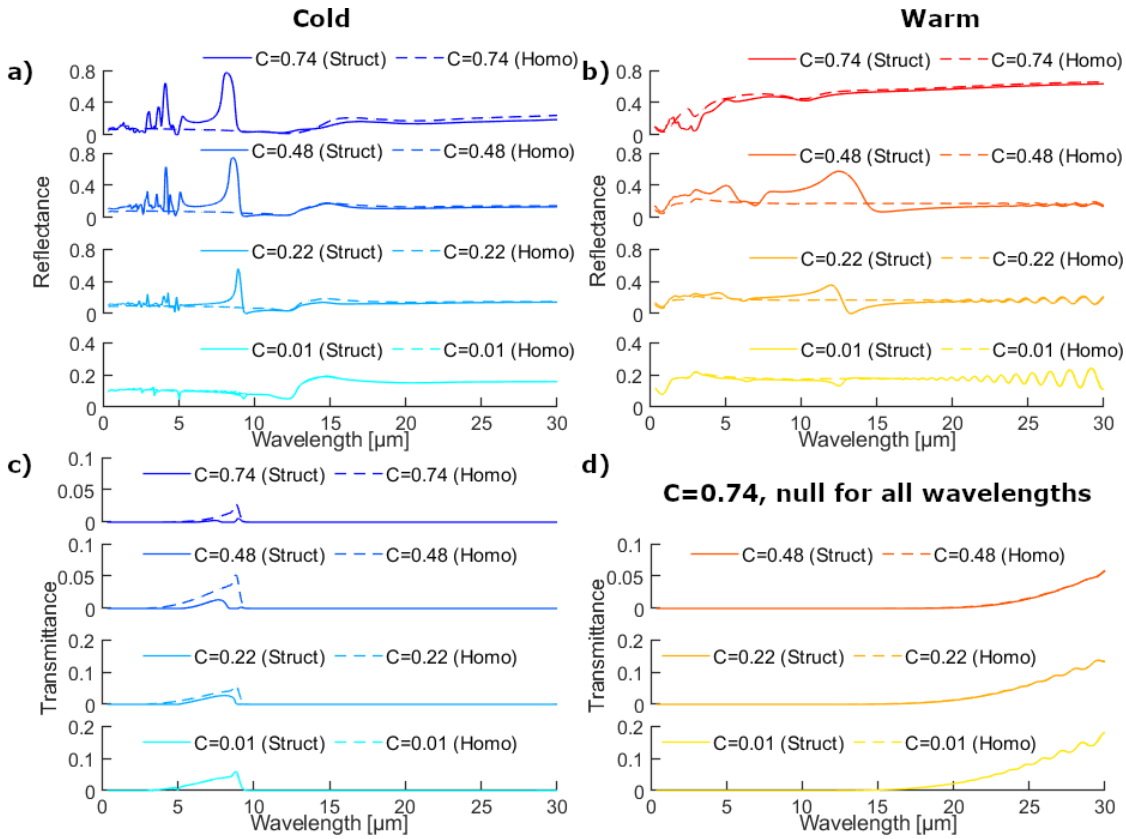

Fig. 4. Reflectance (a), b)) and transmittance (c), d)) spectra of a polymer opal photonic crystal consisting of polymer spheres ($n(P_s) = 1.3$) surrounded by a mixture of VO_2 and another polymer ($n(P_i) = 1.7$) (solid lines, designated by "struct"), and its homogenized counterpart (dashed lines, designated by "homo"), in cold (a)-c)) and warm (b)-d) conditions, for a VO_2 total concentration of 26 vol% and a structure compacity from 0.01 to 0.74 (see Table 1 for the corresponding interstice concentrations). Note that the vertical scale is not the same for all graphs. The transmittance in the case $C = 0.74$ for the warm condition in both homogenized and structured cases is null for all wavelengths. Null means below the computational limit which is 2.22×10^{-16}.

the longest wavelengths due to an increase of the homogenized material effective refractive index real part is also observed.

In the warm conditions, the structure has a very low impact on the reflectance for all wavelengths and all values of f_t. This is due to the high material absorption (see Fig. S4 f)) as well as to the decreasing compacity.

Regarding the transmittance, it only has non-zeros values for $f_t = 26$ vol% in the cold condition, which is the same case previously described in Fig. 4 c) for $C = 0.74$.

B. Emissivity and its modulation

The previously presented reflectance spectra are used to compute the emissivity ϵ (see equation 1) as well as its modulation (see equation 2). The results, for all cases described in Table 1 are presented in Fig. 6.

B.1. Emissivity and its modulation as a function of the total VO_2 concentration f_t

Let's first study the variations of ϵ and $\Delta\epsilon$ as a function of the VO_2 total concentration f_t (see Fig. 6 a)-c)). Looking first at the emissivity values, it can be observed that both for cold and warm conditions and structured and homogenized cases, a first increase of the emissivity is observed, followed by a decrease for f_t higher than about 20 vol%. This decrease is larger in the warm condition. The increase of the emissivity, which is particularly noticeable between 1 vol% and 5 vol%, is due to the important decrease of the material tansmittance, whereas the reflectance doesn't vary a lot (see Fig. 3). With increasing f_t the contribution of the transmittance to the emissivity decreases, starting from a predominant contribution at $f_t = 1$ vol% to an almost negligible contribution for $f_t = 20$ vol%. Whereas homogenized and structured transmittances are close to each other, structured and homogenized reflectances are highly different, mainly because of the PBG and higher order peaks. Correlated with the increasing influence of reflectance, an increasing difference between homogenized and structured cases is observed. Then, for f_t above 20 vol%, the emissivity decrease is due to an increase of the reflectance (see Fig. 5). Whereas structured and homogenized cases have comparable values in the warm condition for f_t above 26 vol%, in the cold case, structured and homogenized cases are comparable for f_t above 78 vol%. This is explained by the absence of PBG peak in the warm condition for f_t above 26 vol% and for f_t above 78 vol% in the cold condition. The PBG peak reduces the emissivity in the structured case compared to the homogeneous one.

Looking at the emissivity modulation, a first slight decrease is observed for f_t between 1 vol% and 10 vol%, followed by a rapid increase and a saturation for f_t above 52 vol%. The rapid increase of $\Delta\epsilon$ is linked to the rapid decrease of the emissivity in the warm condition for f_t above 20 vol%. The main impact of the structure is observed for $f_t = 10$ vol%, with an increase of the emissivity modulation of about 0.08 compared to the ho-

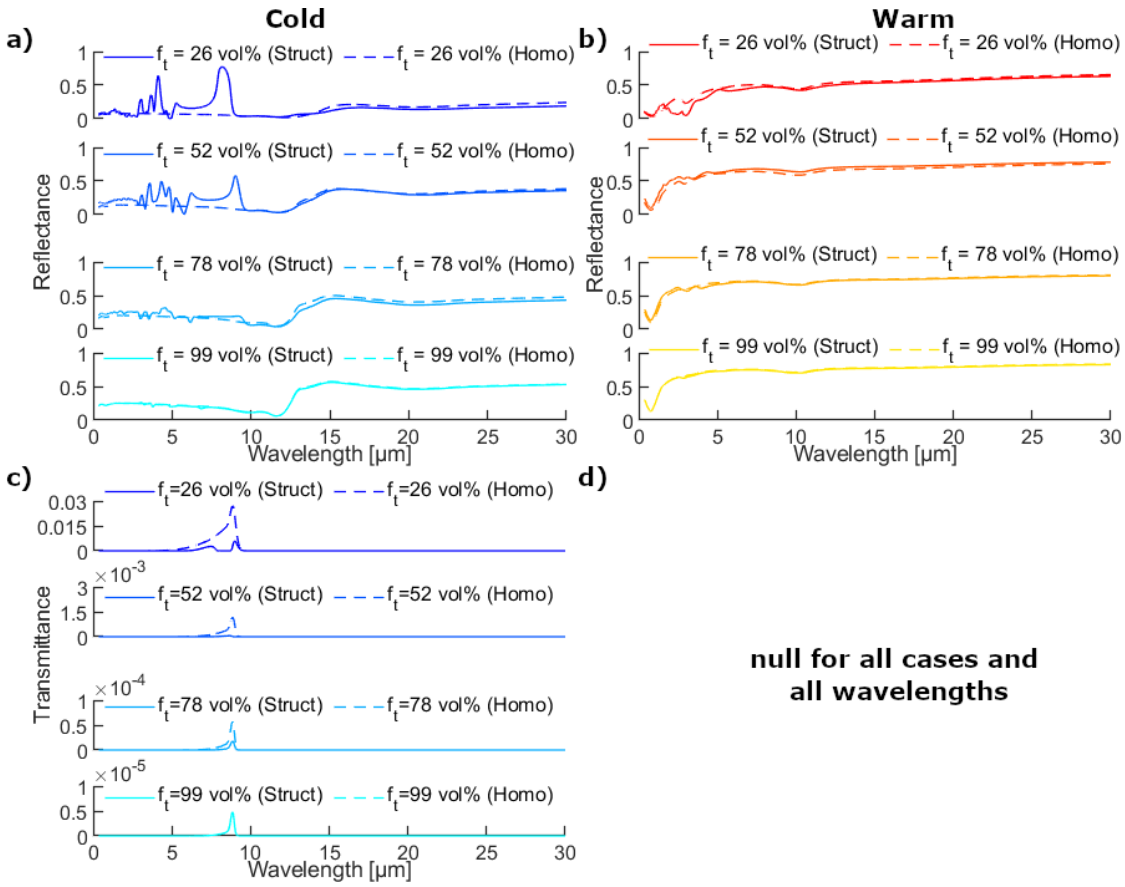

Fig. 5. Reflectance (a), b)) and transmittance (c), d)) spectra of a polymer opal photonic crystal consisting of polymer spheres ($n(P_s) = 1.3$) surrounded by pure VO_2 (solid lines, designated by "struct"), and its homogenized counterpart (dashed lines, designated by "homo"), in cold (a)-c)) and warm (b)-d) conditions, for a VO_2 total concentrations from 26 vol% to 99 vol% and a structure compacity from 0.74 to 0.01 (see Table 1 for the relationship between C and f_t and equation 6). Note that the vertical scale is not the same for all graphs. The transmittance in the warm condition is null for all cases and wavelengths. Null means below the computational limit which is 2.22×10^{-16}.

mogenized case, and for $f_t = 26$ vol%, with an decrease of the emissivity modulation of about 0.1 compared to the homogenized case. For $f_t = 10$ vol%, a high impact of the structure is observed for the emissivity in the warm condition (decrease of the emissivity due to the structure), correlated with a smaller impact in the cold condition, explaining the increase of the emissivity modulation. For $f_t = 26$ vol%, the opposite phenomenon is observed, with a small impact of the structure in the warm condition and a high impact of the structure in the cold condition (decrease of the emissivity), explaining the decrease of the emissivity modulation.

B.2. Emissivity and its modulation as a function of the compacity C

The variations of the emissivity and its modulation as a function of the compacity C are presented in Fig. 6 b)-d). Looking at the emissivity values, a global decrease of the emissivity with the compacity is observed, for both cold and warm conditions. Only the homogenized case in the cold condition exhibits a slight increase with the compacity. In the cold condition, the transmittance has a very low to negligible contribution to the emissivity (see Fig.4). The decrease of ϵ with C is explained in the structured case by the increase of the PBG and higher order reflectance peaks. In the homogenized case, a slight increase of the reflectance with C is observed, leading to a slight increase of ϵ. As expected, the maximum impact of the structure is obtained with the maximum compacity. In the warm condition, the transmittance has low to negligible contribution to the emissivity. The decrease of the emissivity with C in the structured case is explained first by the increase of the PBG (until $C = 0.48$), and then, between $C = 0.48$ and $C = 0.74$, by the global increase of the reflectance values. In the homogenized case, the emissivity remains almost constant for compacities below 0.48, with a rapid decrease between $C = 0.48$ and $C = 0.74$: this is in accordance with the reflectance values, which are almost constant until $C = 0.48$ and exhibit a high increase between $C = 0.48$ and $C = 0.74$.

The emissivity modulation globally increases with C in both the homogenized and structured cases. In the homogenized case, the emissivity modulation remains almost constant for compacities below 0.48, with a high increase between $C = 0.48$ and $C = 0.74$: this is due to the constant values of the cold and warm emissivity below $C = 0.48$ and the rapid decrease of the warm emissivity between $C = 0.48$ and $C = 0.74$. In the structured case, a more steady increase of $\Delta\epsilon$ with C is observed, due to the more pronounced decrease of the warm emissivity than this of the cold one.

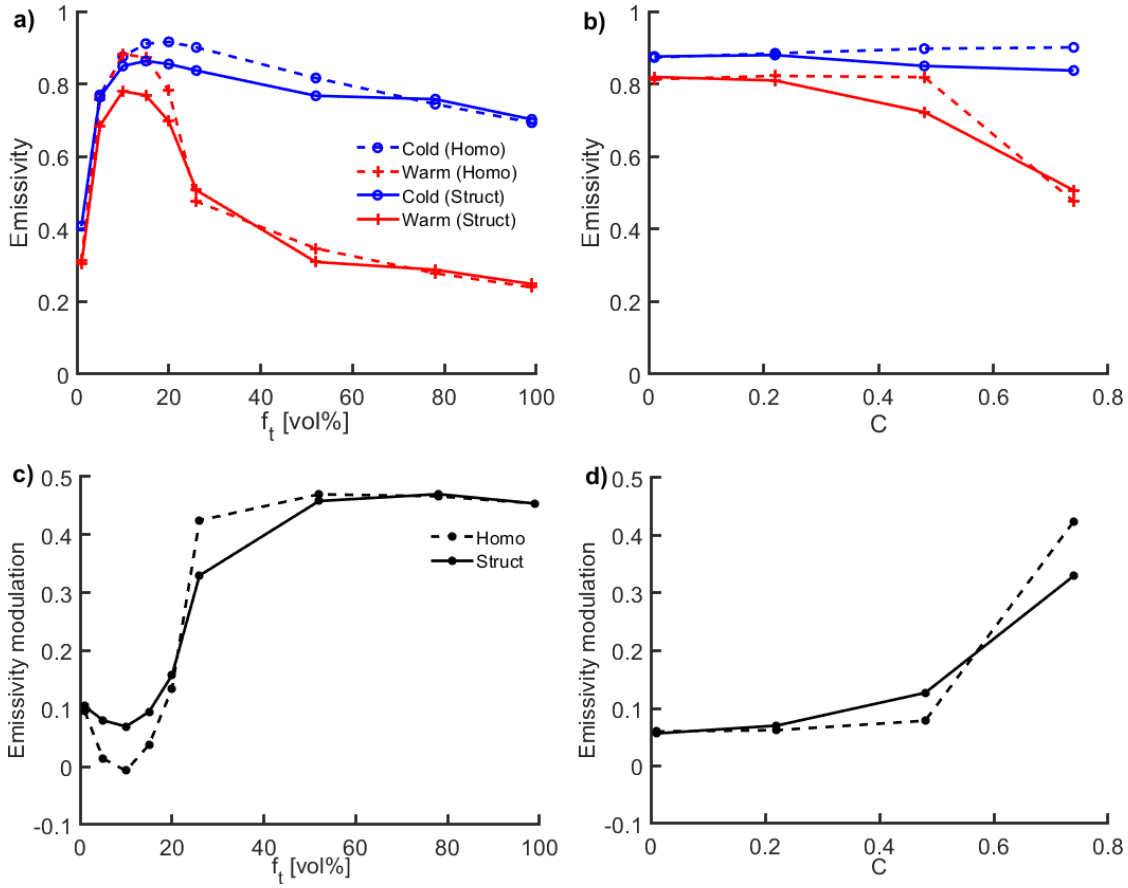

Fig. 6. Calculated emissivity ϵ (a), b)) and its modulation $\Delta\epsilon$ (c), d)) of an opal photonic crystal consisting of polymer spheres ($n(P_s) = 1.3$) surrounded by a mixture of VO_2 and another polymer ($n(P_i) = 1.7$) (solid lines), and its homogenized counterpart (dashed lines), as a function of VO_2 total concentration (a), c)) and structure compacity in the case where the total VO_2 concentration is equal to $f_t = 26$ vol%.

4. CONCLUSION

The optical and thermal properties of a polymer opal photonic crystal containing VO_2 nanoparticles in the opal interstices are studied. Structural parameters were chosen in order to maximize the impact of the PBG on the material emissivity. With a cell parameter a = 4.5 µm and 15 periods in the [111] direction (thickness of 117 μm), a strong PBG effect can occur in the mid-IR, where the blackbody emittance peak at a temperature of τ = 70°C (approximate temperature of the VO_2 phase transition) is located. This reflectance peak leads to reduced emissivities compared to the homogenized material, with a maximum decrease of about 0.06 in the cold case ($f_t = 20$ vol% and $f_t = 26$ vol% with $C = 0.74$) and of about 0.1 in the warm case ($f_t = 10$ vol% and $f_t = 15$ vol% with $C = 0.74$). If this decrease occurs mainly in the warm case, it is accompanied by an increase of the emissivity modulation (f_t from 5 vol% to 15 vol% and $C = 0.74$). This increase could be useful for camouflage applications, in the cases where low VO_2 total concentrations are required. VO_2 is black and low VO_2 concentrations are interesting for paints, when light colors are required, for example to avoid too high absorption of the sun light in the visible wavelength range. Nevertheless, when a maximum emissivity modulation is necessary for camouflage applications, regardless of the material color, the highest VO_2 concentrations have the best performances, with no impact of the material structure. For a VO_2 total concentration higher than 52 vol%, $\Delta\epsilon$ varies around values from 0.45 to 0.47. This is comparable to the $\Delta\epsilon$ = 0.46 measured on VO_2 nanopowder pellets by Ji et al. [1]. Ono et al. [13] obtained a theoretical emissivity modulation in the wavelength range [8 µm - 14 µm] of about 0.57. In this wavelength range, the emissivity modulation in our case varies from 0.51 to 0.55 for f_t above 52 vol% in the homogenized or structured cases (see Fig. S6), which remains comparable. At these high VO_2 concentrations, the structure does not have much effect on the material emissivity as the material is more absorbent, which reduces the PBG amplitude.

Regarding applications like energy-efficient coatings for buildings and satellites where a negative emissivity modulation is required, an optimized case for this application would be for a VO_2 concentration of 10 vol%. However, the structure has a negative impact in this case, as it tends to increase $\Delta\epsilon$. The lowest emissivity modulation is -0.007 (homogeneous case for $f_t = 10$ vol%), which is a poor performance compared to putting a VO_2 film above a low emissivity substrate. Benkahoul et al. [6] obtained for example an emissivity modulation of -0.26 for a VO_2/Al system. Various publications obtained far better performances in the [8 µm - 14 µm] wavelength range, for example [8–10, 13] with theoretical emissivity modulations of respectively -0.73, -0.80, -0.83, -0.54 or [14, 15] with experimental emissivity modulations of respectively -0.62 and -0.67, with VO_2 for the first ones and $Ge_2Sb_2Te_5$ for the two latter ones. The best neg-

ative emissivity modulation in the [8 µm - 14 µm] wavelength range is in our case -0.05 for $f_t = 5$ vol% in the homogenized case (see Fig. S6).

This paper confirms the good performance of VO_2/polymer nanocomposites for camouflage applications, whereas it is less interesting for energy-efficient coatings. Structuring the polymer has a weak effect, but a perfectly ordered structure is assumed here, which can differ from experimental opals where disorder could modify this impact.

5. BACKMATTER

Funding.

Acknowledgments. This work has been funded by La Région Auvergne-Rhône-Alpes and supported by the LABEX MANUTECH-SISE (ANR-10-LABX-0075) of Université de Lyon, within the program "Investissements d'Avenir" (ANR-11-IDEX-0007) operated by the French National Research Agency (ANR) and ANR Thermocoat (ANR-16-CE22-0014).

Disclosures. The authors declare no conflicts of interest.

Data availability. Data underlying the results presented in this paper are not publicly available at this time but may be obtained from the authors upon reasonable request.

Supplemental document. See Supplement 1 for supporting content.

REFERENCES

1. H. Ji, D. Liu, H. Cheng, C. Zhang, and L. Yang, "Vanadium dioxide nanopowders with tunable emissivity for adaptive infrared camouflage in both thermal atmospheric windows," Sol. Energy Mater. Sol. Cells **175**, 96–101 (2018).
2. L. Xiao, H. Ma, J. Liu, W. Zhao, Y. Jia, Q. Zhao, K. Liu, Y. Wu, Y. Wei, S. Fan *et al.*, "Fast adaptive thermal camouflage based on flexible vo2/graphene/cnt thin films," Nano letters **15**, 8365–8370 (2015).
3. H. Ji, D. Liu, C. Zhang, and H. Cheng, "Vo2/zns core-shell nanoparticle for the adaptive infrared camouflage application with modified color and enhanced oxidation resistance," Sol. Energy Mater. Sol. Cells **176**, 1–8 (2018).
4. M. A. Kats, R. Blanchard, S. Zhang, P. Genevet, C. Ko, S. Ramanathan, and F. Capasso, "Vanadium dioxide as a natural disordered metamaterial: Perfect thermal emission and large broadband negative differential thermal emittance," Phys. Rev. X **3**, 1–7 (2014).
5. D. Liu, H. Ji, R. Peng, H. Cheng, and C. Zhang, "Infrared chameleon-like behavior from VO2(M) thin films prepared by transformation of metastable VO2(B) for adaptive camouflage in both thermal atmospheric windows," Sol. Energy Mater. Sol. Cells **185**, 210–217 (2018).
6. M. Benkahoul, M. Chaker, J. Margot, E. Haddad, R. Kruzelecky, B. Wong, W. Jamroz, and P. Poinas, "Thermochromic vo2 film deposited on al with tunable thermal emissivity for space applications," Sol. Energy Mater. Sol. Cells **95**, 3504–3508 (2011).
7. W. J. Kort-Kamp, S. Kramadhati, A. K. Azad, M. T. Reiten, and D. A. Dalvit, "Passive Radiative "thermostat" Enabled by Phase-Change Photonic Nanostructures," ACS Photonics **5**, 4554–4560 (2018).
8. M. Ono, K. Chen, W. Li, and S. Fan, "Self-adaptive radiative cooling based on phase change materials," Opt. Express **26**, A777 (2018).
9. W.-W. Zhang, H. Qi, A.-T. Sun, Y.-T. Ren, and J.-W. Shi, "Periodic trapezoidal VO 2 -Ge multilayer absorber for dynamic radiative cooling," Opt. Express **28**, 20609 (2020).
10. S.-H. Wu, M. Chen, M. T. Barako, V. Jankovic, P. W. Hon, L. A. Sweatlock, and M. L. Povinelli, "Thermal homeostasis using microstructured phase-change materials," Optica **4**, 1390 (2017).
11. K. Sun, C. A. Riedel, A. Urbani, M. Simeoni, S. Mengali, M. Zalkovskij, B. Bilenberg, C. De Groot, and O. L. Muskens, "Vo2 thermochromic metamaterial-based smart optical solar reflector," ACS photonics **5**, 2280–2286 (2018).
12. A. Hendaoui, N. Émond, S. Dorval, M. Chaker, and E. Haddad, "Vo2-based smart coatings with improved emittance-switching properties for an energy-efficient near room-temperature thermal control of spacecrafts," Sol. energy materials solar cells **117**, 494–498 (2013).
13. M. Ono, M. Takata, M. Shirata, T. Yoshihiro, T. Tani, M. Naya, and T. Saiki, "Self-adaptive control of infrared emissivity in a solution-processed plasmonic structure," Opt. Express **29**, 36048 (2021).
14. K. Du, Q. Li, Y. Lyu, J. Ding, Y. Lu, Z. Cheng, and M. Qiu, "Control over emissivity of zero-static-power thermal emitters based on phase-changing material GST," Light. Sci. Appl. **6**, e16194 (2017).
15. Y. Qu, Q. Li, L. Cai, M. Pan, P. Ghosh, K. Du, and M. Qiu, "Thermal camouflage based on the phase-changing material GST," Light. Sci. Appl. **7**, 1–10 (2018).
16. J.-L. Meyzonnette and T. Lépine, *Bases de radiométrie optique* (Cépaduès, Toulouse, 1999).
17. L. Kang, Y. Gao, Z. Chen, J. Du, Z. Zhang, and H. Luo, "Pt/vo2 double-layered films combining thermochromic properties with low emissivity," Sol. energy materials solar cells **94**, 2078–2084 (2010).
18. B. Baloukas, S. Loquai, and L. Martinu, "Vo2-based thermally active low emissivity coatings," Sol. Energy Mater. Sol. Cells **183**, 25–33 (2018).
19. Y. Guo, B. Xiong, Y. Shuai, and J. Zhao, "Thermal driven wavelength-selective optical switch based on magnetic polaritons coupling," J. Quant. Spectrosc. Radiat. Transf. **255**, 107230 (2020).
20. J. Faucheu, E. Bourgeat-Lami, and V. Prevot, "A review of vanadium dioxide as an actor of nanothermochromism: challenges and perspectives for polymer nanocomposites," Adv. Eng. Mater. **21**, 1800438 (2019).
21. https://www.np.phy.cam.ac.uk/research-themes/polymer-opals.
22. O. L. Pursiainen, J. J. Baumberg, H. Winkler, B. Viel, P. Spahn, and T. Ruhl, "Nanoparticle-tuned structural color from polymer opals." Opt. express **15**, 9553–9561 (2007).
23. J. D. Joannopoulos, S. G. Johnson, J. N. Winn, and R. D. Meade, *Photonic Crystals: Molding the Flow of Light* (Princeton University Press, 2008), 2nd ed.
24. L. Li, *Fourier Modal Method* (Gratings: Theory and Numeric Applications, Second Revisited Edition, Aix Marseille Université, 2014).
25. "Mc grating software," https://mcgrating.com/.
26. V. A. Markel, "Introduction to the maxwell garnett approximation: tutorial," JOSA A **33**, 1244–1256 (2016).
27. E. Popov, M. Nevière, B. Gralak, and G. Tayeb, "Staircase approximation validity for arbitrary-shaped gratings," JOSA A **19**, 33–42 (2002).
28. N. R. Mlyuka, G. A. Niklasson, and C. G. Granqvist, "Thermochromic vo2-based multilayer films with enhanced luminous transmittance and solar modulation," physica status solidi (a) **206**, 2155–2160 (2009).
29. G. Mayonado, S. M. Mian, V. Robbiano, and F. Cacialli, "Investigation Of The Bragg-Snell Law In Photonic Crystals," in *BFY Proceedings,* (2015), pp. 60–63.
30. A. Beer, "Bestimmung der Absorption des rothen Lichts in farbigen Flüssigkeiten," Annalen der Physik und Chemie **86**, 78–88 (1852).
31. J.-H. Lambert, *Photometria, sive de mensura et gradibus luminis, colorum et umbrae* (C.P. Detleffsen, 1760).
32. P. Bouguer, *Essai d'optique sur la gradation de la lumière* (Jombert, Claude, Paris, 1729).